Energy Conversion Circuit Laboratory

Power Factor Control Scheme for Zero Current Harmonics of Battery Charger in EVs

Cong-Long Nguyen*, Hong-Hee Lee†, and Sung-Jin Choi*

† * School of Electrical Engineering, University of Ulsan, Ulsan, Korea
hhlee@mail.ulsan.ac.kr

***Abstract*-The input current harmonics of battery chargers affect harmfully on the overall power distribution network. They result in voltage distortion, heating transformers, reducing conduction capacity of cable, and affecting the interrupting capability of circuit breakers. In order to eliminate these problems, this paper presents an effective control scheme to remove input current harmonics of battery charger by controlling the current in phase with fundamental component of the grid voltage. The proposed control scheme not only achieves near-unity input power factor but also eliminates current harmonics in the battery charger regardless of the grid voltage disturbance. To validate performance of the proposed control scheme, both simulation and experiment are carried out.**

Keywords: Electric vehicles (EVs), battery charger, digital control, power quality, total harmonic distortion (THD).

I. INTRODUCTION

To solve the acute global problems such as environmental pollution and crisis of energy source, electric vehicles (EVs) become one of the most promising candidates to replace the current petroleum-based vehicular system [1]. In developed countries, by year 2050, it is estimated that at least 50% of vehicles in the road could be electric types, which are electrically powered from the grid system at home or at public charging station via battery chargers [2]. Hence, in near future, an enormous number of EVs battery chargers will be plugged in the distribution system that lead to the increasing of the power generation and impact on the power quality [3], [4]. Among these impacts, recent studies showed that the additional electric energy required by EVs is not a critical problem [5]. In contrast, harmonics current drawing from battery chargers to the grid causes serious issues such as distorting the grid voltage, heating distribution transformers, and reducing cables conduction capacity [4]. Thus, battery chargers must be designed carefully to reduce the input current harmonics, which helps the distribution system prevent those severe effects.

To fulfill that requirement, battery charger manufacturers have been upgrading new designs, which usually require a front-end power-factor-corrected (PFC) converter. Compared with old designs that commonly based on full-wave uncontrolled diode rectifiers or ferro-resonant transformers [6], the new designs enhance power factor (PF) to be near-unity and reduce total harmonic distortion (THD) of input current significantly. Fig.1 illustrates a practical charging system with employing a front-end PFC boost converter. The system is similar to topologies discussed in [7]. As a vehicle parked and charged, power is transferred from a utility to a battery bank through a high frequency inductive coupling, which leads to a maximum operator safety. In this charging system, to charge the battery bank with desired charging algorithm, voltage and current of the dc-link must be regulated at predetermined values. Hence, controlling the charging system now turns into controlling the PFC boost converter as shown in Fig. 2. The load in this figure has behavior like the battery bank in the vehicle. In order to control the PFC boost converter for achieving unity power factor and a desired charging algorithm, a control scheme was introduced in [8]. This control scheme consists of two outer controllers to implement a charging algorithm and an inner current controller to control the grid (input) current waveform. However, the paper only focuses on the outer controllers. The current controller is briefly mentioned and uses a proportional-integral (PI) regulator to regulate the grid current in phase with the grid voltage. Thus, this control approach may result in the grid current distorted if the grid voltage contains disturbance.

In this paper, a new control scheme for the charging system is proposed. Under this control scheme, the battery charger injects zero-harmonics current to the utility regardless of the grid voltage distortion. The main idea of the proposed control scheme is to control the grid current in phase with a pure sinusoidal waveform that is the fundamental component of the grid voltage. To detect this waveform, a band-pass filter (BPF) and a phase-locked loop (PLL) are designed. Furthermore, with utilizing feed-forward paths in both the current control algorithm and charging control algorithm, the grid current is able to track its desirable waveform perfectly and dynamic performance of the overall system is enhanced significantly. In order to verify effectiveness of the proposed control scheme, both simulation and experiment are carried out.

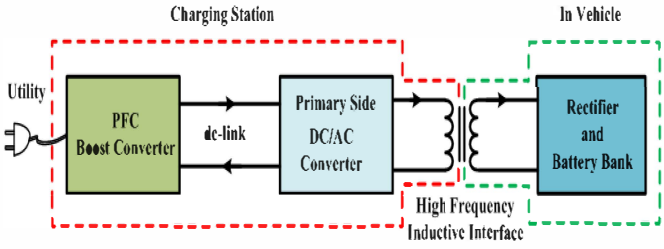

Fig. 1. Battery charging system overview.

978-1-4673-0954-7/12/$31.00 ©2012 IEEE

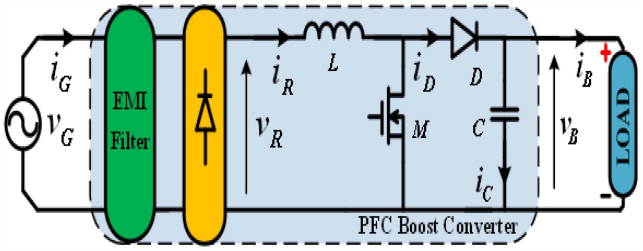

Fig. 2. PFC boost converter.

II. THE POWER FACTOR CORRECTED BOOST CONVERTER

The configuration of PFC boost converter is illustrated in Fig. 2, which consists of a full-bridge diode rectifier, a step-up dc chopper with energy storage elements, and an electromagnetic interference (EMI) filter. Due to advantage characteristics such as simple construction, small size, low cost and high efficiency, this converter has been widely adopted to comply with regulations of low input current harmonic distortion [9]. In general applications, which have only a single operating point (i.e. the dc output voltage demands to be kept at a desired constant value), the switch M is usually regulated through a simple controller like peak current control, average current control or hysteresis current control. However, in tracking application such as battery charger, there may be no a single nominal operating point for the converter (i.e. the dc output voltage or current must be followed a desired reference waveform as a function of time), thus the system controller needs to provide stable well-characterized performance in the presence of large-signal variations. In this section, the model of the PFC boost converter is described via some key mathematic equations, which are essential to propose an effective control strategy for the converter utilized to the battery charging application.

In order to model the behaviors of the PFC boost converter, some assumptions are initially made: 1) the converter elements are ideal and thus, lossless. 2) The switching frequency f_S is infinite as compared with the grid frequency f_G. 3) The output capacitor C is large enough to maintain the output dc voltage v_B constant. 4) The input power factor is unity, hence, if the grid voltage is defined $v_G(t) = V_P \sin(\omega t)$, the grid current will be $i_G(t) = I_P \sin(\omega t)$.

Based on the above assumptions and the instantaneous power conservation law, the following equation is achieved

$$p_I(t) = v_G(t) i_G(t) = p_O(t) = v_B(t) i_D(t) \tag{1}$$

where $p_I(t)$ and $p_O(t)$ are the instantaneous input and output power, respectively; and $i_D(t)$ is the diode current. From (1), if the average value of the output voltage and the load current within one grid period are denoted correspondingly as V_B and I_B, the peak input current can be expressed

$$I_P = \frac{2V_B I_B}{V_P}. \tag{2}$$

Due to the bulk output capacitor C, the output voltage v_B is supposed to be its averaged value V_B. Therefore, the diode current i_D can be derived as following

$$i_D(t) = \frac{p_I(t)}{V_B} = \frac{V_P I_P}{2V_B} - \frac{V_P I_P}{2V_B}\cos(2\omega t) = I_B + i_C(t) \tag{3}$$

where $i_C(t)$ is the ac current through the output capacitor C and it is expressed

$$i_C(t) = -\frac{V_P I_P}{2V_B}\cos(2\omega t) = -I_B \cos(2\omega t). \tag{4}$$

During turning on the switch within a time interval t_{ON}, the inductor L is short-circuited so its current will be charged with a quantity

$$\Delta i_{ON} = \frac{1}{L}\int_{t}^{t+t_{ON}} |v_G(\tau)|\, d\tau. \tag{5}$$

Meanwhile, the inductor current will be discharged when the switch turns off and the current decrement amount is

$$\Delta i_{OFF} = \frac{1}{L}\int_{t+t_{ON}}^{t+T_S} \{v_B(\tau) - |v_G(\tau)|\}\, d\tau \tag{6}$$

where T_S is the switching period or $T_S = 1/f_S$. Considering that the converter is operating at the boundary of continuous conduction mode (CCM) and discontinuous conduction mode (DCM), the inductor current charging and discharging amount in a period should be same i.e. $\Delta i_{ON} = \Delta i_{OFF}$. By equating and integrating (5) and (6), the duty ratio can be expressed in this case as

$$d(t) = \frac{t_{ON}}{T_S} = 1 - \frac{|v_G(t)|}{v_B(t)}. \tag{7}$$

III. BATTERY CHARGING ALGORITHM

Fig. 3 illustrates generally the proposed control scheme, which is composed of two cascading blocks named charging control algorithm and current control algorithm. Both of them will be discussed in detail in this section and next section. As shown in Fig.3, the proposed control scheme is implemented in a digital signal processor (DSP). Therefore, all control variables (the battery voltage v_B, the battery current i_B, the grid voltage v_G, and the rectified input current i_R) are converted into digital quantities by using measurement circuits (T_0-T_3) and analog-to-digital converters (ADC).

The objective of charging control strategy is to maintain the battery voltage and the battery current at their desired reference waveform to ensure the battery is charged with an installed charging method. In Fig. 4(a), a popular charging algorithm called constant-current constant-voltage (CC-CV)

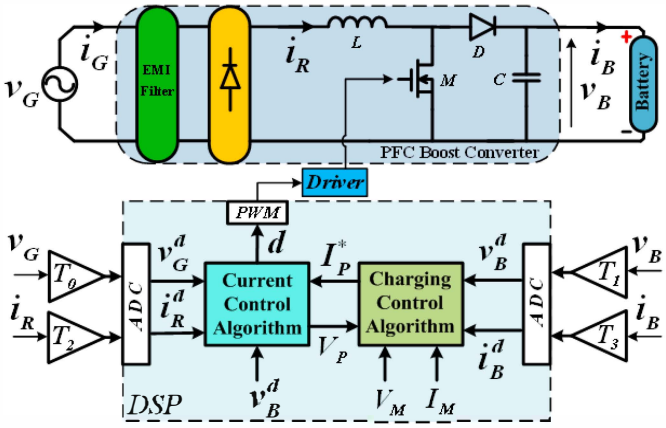

Fig. 3. The proposed control scheme in general.

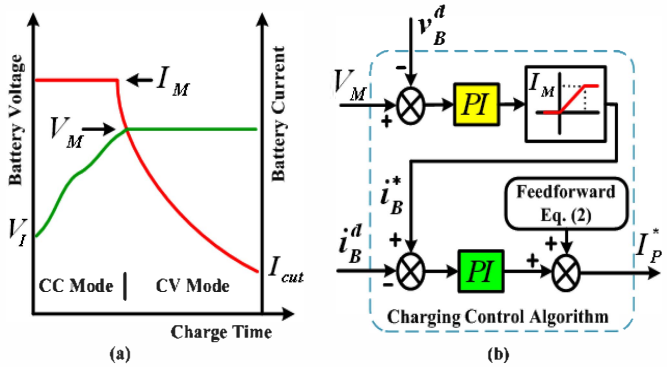

Fig. 4. (a) CC-CV charging method. (b) The proposed charging control algorithm.

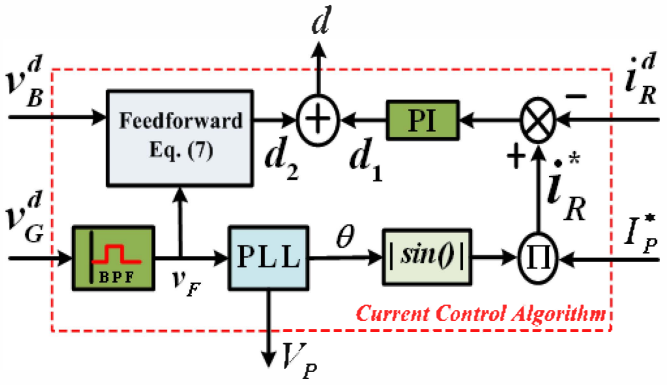

Fig. 5. The proposed current control algorithm.

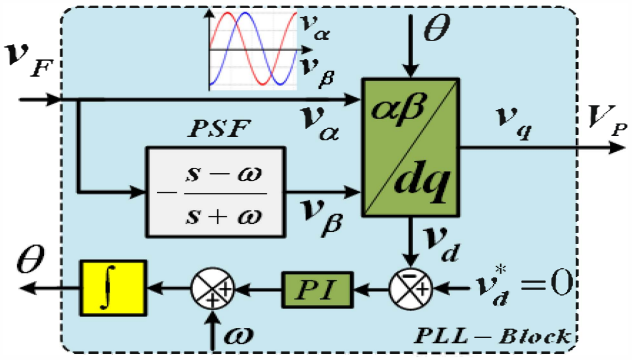

Fig. 6. The single phase PLL technique.

method is shown. It is usually used to charge lithium-ion, lead-acid or some other batteries that are vulnerable to damage if an upper voltage limit V_M is exceeded. To reduce charge time, in CC mode, the charging current should be maintained at a rating I_M. When the battery voltage reaches the limit V_M, the charging mode shifted to CV mode to keep the battery voltage at that level. During the CV mode, the charging current decreases to a predetermined cut-off current point I_{cut}, which indicates the battery is full charge. Noted that the voltage limit V_M, the rating current I_M, and the cut-off current I_{cut} are determined from the battery specification. In this paper, the charging technique is implemented to the charging system by the proposed control scheme shown in Fig. 4(b), where two PI controllers are used for controlling CC and CV mode. The first controller regulates the battery charging voltage by mean of generating a charging current reference for the second controller. In order to ensure the charging process not over-current, this reference signal should be limited at I_M by a saturation block. As mentioned earlier, in a tracking application like battery charger, the control strategy must manage the battery voltage and the charging current to follow their reference waveforms stringently. It means that dynamic response and steady state error performance are two criterions to evaluate the benefits of the control strategy. In this paper, to enhance these performances, a feed-forward component is added to the output of the second PI controller. Because the charging control algorithm determines the grid current amplitude I_P^*, the feed-forward here should execute the expression defined in (2). Noted that the grid voltage amplitude V_P in this equation is obtained from an output of the PLL block, which will be discussed within next section.

IV. CURRENT CONTROL ALGORITHM

The proposed current control algorithm as shown in Fig. 5 is an inner part of the overall control scheme (Fig. 3). For the aim of removing input current harmonics, the grid current i_G is controlled to be in phase with only fundamental component of the grid voltage. It helps the input current is undisturbed although the ac utility voltage contains disturbance. In order to detect the fundamental component v_F without effecting its phase, a second band pass filter (BPF) with a center frequency coinciding to the grid frequency is selected. Therefore, transfer function of the filter is defined as

$$H(s) = \frac{bs}{s^2 + bs + \omega^2} \tag{8}$$

where ω is the center frequency of the filter ($\omega = 120\pi$ rad/s), b is a band-width of the filter and chose to one-tenth of the center frequency ($b = 12\pi$ rad/s). Subsequently, phase of the fundamental voltage is determined by using a PLL technique as shown in Fig. 6. It is a single-phase PLL technique imitating three-phase PLL methods [10]. A virtual $\pi/2$ phase-lag voltage v_β compared with v_F is obtained by using a first-order 90-degree-phase-shift function (PSF) that is

$$P(s) = -\frac{s-\omega}{s+\omega}. \quad (9)$$

At the line frequency ω, the output signal of this function is lagged an angle of $\pi/2$ and has same magnitude in comparison with its input signal. Afterwards, v_α and v_β are changed to the direct quantities v_d and v_q by the Park Transform as following equations

$$\begin{bmatrix} v_d \\ v_q \end{bmatrix} = \begin{bmatrix} \cos\theta & \sin\theta \\ -\sin\theta & \cos\theta \end{bmatrix} \begin{bmatrix} v_\alpha \\ v_\beta \end{bmatrix}. \quad (10)$$

If angle θ in (10) is the phase of v_α (i.e. phase of v_F), then v_d will be zero and v_q will be a peak value of v_F. So, a PI controller is used to control v_d component to be zero as drawn in Fig. 6. The output of this controller adding to the line frequency ω is integrated to compute the phase of the grid voltage eventually.

As mentioned earlier, the current control algorithm shown in Fig. 5 holds a task of regulating the input current to follow a desirable waveform that is matching phase with the fundamental component of the grid voltage and has amplitude decided by the charging control algorithm. In order to accomplish this task, a feed-forward path and a PI compensator are employed. Actually, if the controller is implemented through an analog circuit, the controller bandwidth will be high enough to provide a good performance. On the other hand, digital implementation through the DSP has some limitations for the PI compensator due to the lower sampling time and switching frequency compared with that of the analog controller. Therefore, in the digital control, the feed-forward path is indispensable to improve the input current performance as being without phase displacement compared with its reference. In this paper, a duty feed-forward control is used and it is defined in (7).

V. SIMULATION AND EXPERIMENTAL RESULTS

In order to verify the effectiveness of the proposed control scheme, simulation and experiment are carried out. The converter is setup in a laboratory and used to charge a $72V$-$50Ah$ seal lead-acid battery bank. The overall charging system as shown in Fig. 7 is developed with a high performance DSP (TMS320F28335 by Texas Instruments). To insure the PFC boost converter operation, the grid voltage has been scaled down to $50V/60Hz$ through a programmable ac source. In addition, for simulation purpose, the battery is modeled by an equivalent circuit introduced in [11] and a PSIM software by POWERSIM Inc. is utilized.

Table I lists main power components used in the $1kW$ experimental prototypes. Additionally, the EMI filter utilizes only a $1\mu F$ metalized polypropylene film capacitor and the MOSFET M is controlled and switched at 50 KHz. In both simulation and experiment, the battery bank has specifications as shown in Table II.

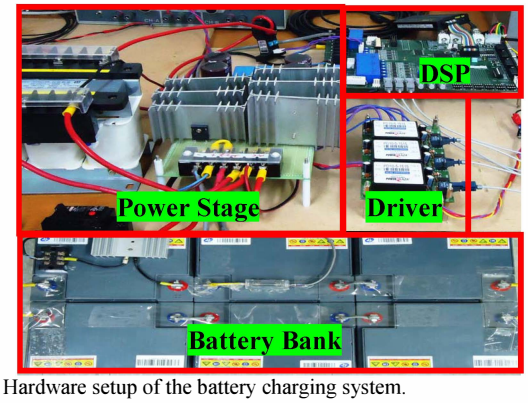

Fig. 7. Hardware setup of the battery charging system.

TABLE I
KEY COMPONENTS USED IN THE CHARGING SYSTEM

Devices	Part # / Value
Mosfet/Diode: M/D	IRFP460/RURG8060
Full-bridge Diode Rectifier	Two Modules: VSKD56
Smoothing Capacitor/Inductor: C/L	8.8 mF/1.05 mH
Driver	HCPL-3120
Voltage Transducer: T_0/T_1	LEM LV 25-P
Current Transducer: T_2/T_3	LEM HX 30-P

TABLE II
PARAMETER VALUES OF THE BATTERY BANK

Battery Model	NEWMAX PNC 12500	
Nominal Voltage	12V	
Typical Capacity	50Ah	
Charge Condition	Max. Current	16A
	Max. Voltage	14.4 ~ 15.0V
Battery Bank Construction (12[V]x6=72[V])	Internal Resistance	48 $m\Omega$
	Charging Current	16A
	Cut-off Current	2A
	Max. Voltage	86V

Comparing with the conventional control scheme, this study has some innovative points that are: 1) in the charging control algorithm, the voltage feed-forward component is added. 2) The input current is controlled to be in phase with only fundamental component of the grid voltage. 3) The duty feed-forward path is applied to the current control algorithm. In order to highlight value of this proposed control strategy, the charging system is tested by using both conventional and proposed control algorithms.

The simulation results of the conventional scheme and the proposed control scheme are shown in Fig. 8 and Fig. 9, respectively. In both figures, three signals including the grid voltage, the grid current and the charging current waveform are plotted out from top to bottom. The $50V/60Hz$ grid voltage contains a fifth-order harmonic leading to THD = 6%. It is clear to recognize that the grid current regulated by the conventional control scheme (Fig. 8) is highly distorted with THD=8.1%. Meanwhile, the grid current controlled by the

proposed control algorithm performs as a pure sinusoidal waveform and matching phase with fundamental component of the grid voltage so that a near unity input power factor is achieved (PF=0.998).

The PLL technique performances in the experimental system are shown in Fig. 10. The peak voltage and the phase of fundamental component of the grid voltage are detected successfully.

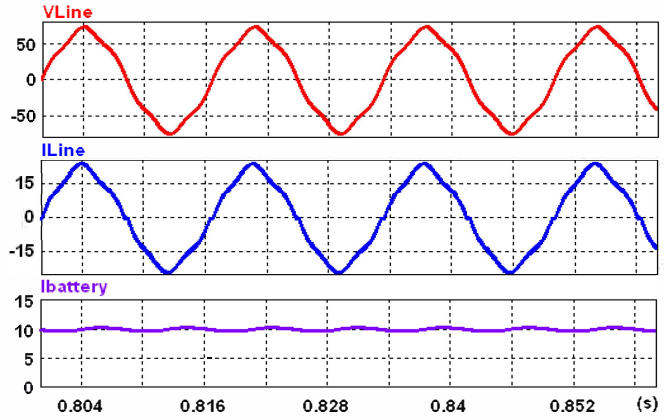

Fig. 8. Simulation results of the conventional control scheme. From top to bottom, the 50V/60Hz grid voltage containing 6% fifth-order component, the grid current and charging current are shown.

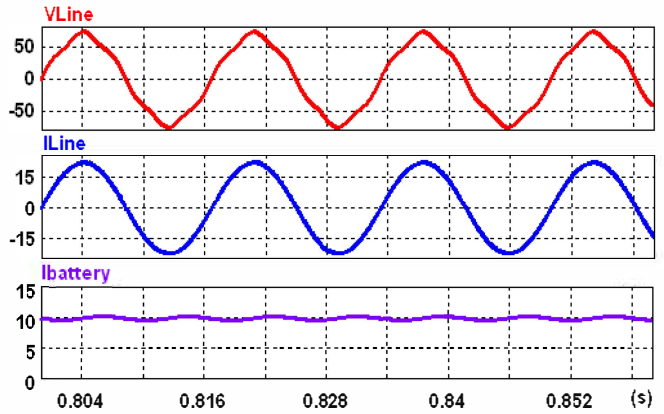

Fig. 9. Simulation results of the proposed control scheme. From top to bottom, the 50V/60Hz grid voltage containing 6% fifth-order component, the grid current and the battery charging current are plotted.

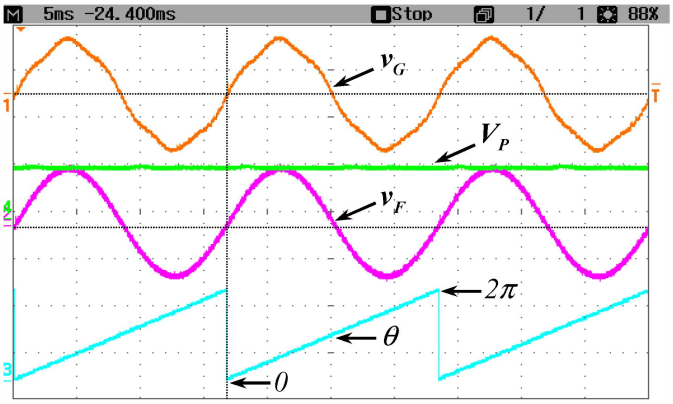

Fig. 10. The PLL technique performance. From top to bottom, the $50V/60Hz$ grid voltage v_G , the peak voltage V_P of grid voltage, the grid voltage fundamental component v_F , and the phase θ of v_F are illustrated.

The improvement of the proposed control scheme in experiment is figured out obviously when comparing the experimental results of the conventional scheme as shown in Fig. 11 with that of the proposed control algorithm illustrated in Fig. 12. Both experiments are used to charge the battery bank at $83V$ and $9A$-charging current. Although it is same grid voltage condition ($50V/60Hz$ with 6% fifth-order harmonic), the grid current regulated by the proposed control scheme is a sinusoidal waveform meanwhile the grid current managed by the conventional scheme is largely distorted (THD=8.17%).

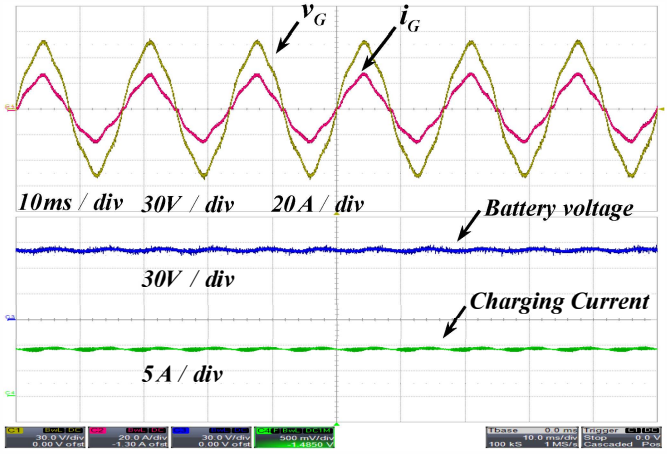

Fig. 11. Experimental results of the conventional control scheme.

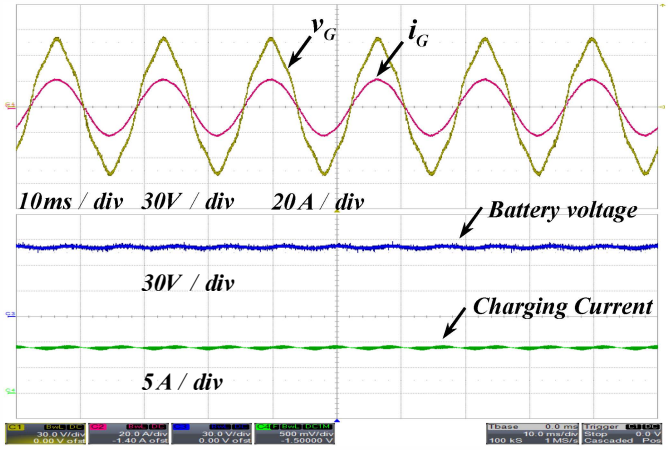

Fig. 12. Experimental results of the proposed control scheme.

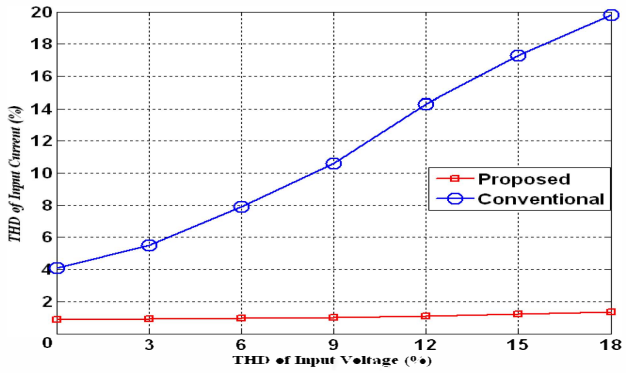

Fig. 13. Comparative results in THD of grid current.

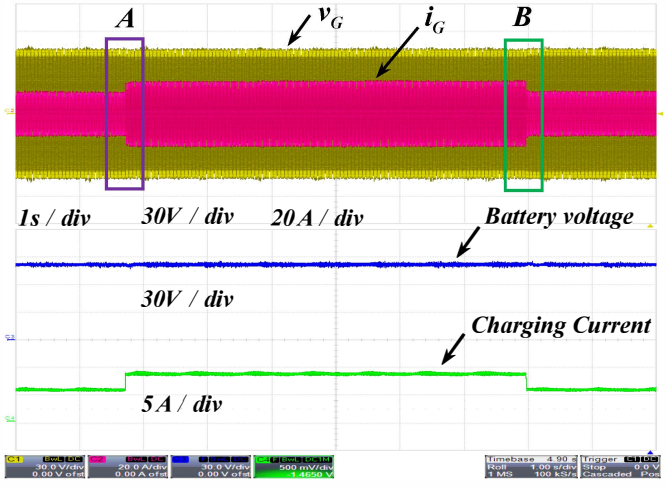

(a)

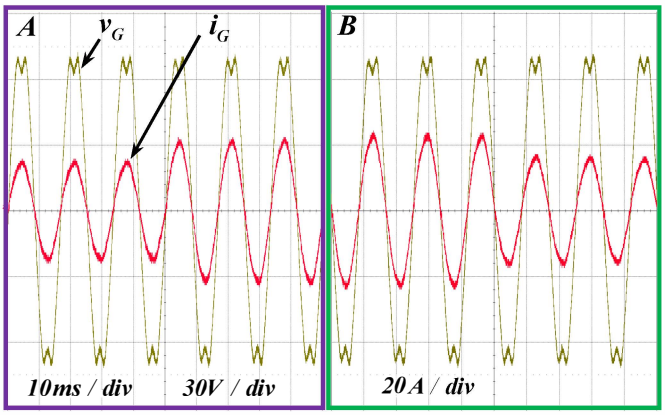

(b)

Fig. 14. (a) Testing dynamic response of the proposed controls scheme. (b) Zooming in at A and B regions within Fig. 14a where charging current command is changed.

The charging system is tested under several grid voltage conditions with conventional and proposed control scheme whose results are shown in Fig. 13. It is easy to observe that the THD of the grid current in the conventional control scheme increases proportionally to THD of the grid voltage caused by the fifth-order harmonic. On the contrary, the grid current performed by the proposed control scheme is near-zero THD and regardless of grid voltage circumstances, proving the value of the proposed control algorithm.

In order to test dynamic response of the proposed control scheme, the charging current command is alternated between 5*A* and 9*A* within 6*s* and the system performances are illustrated in Fig. 14. It is noted that the grid voltage in this test is highly distorted with THD equals to 9.2% by some common odd-order harmonics including third order (8%), fifth order (4%), and seventh order harmonic (2%). At the times of altering the charging current command, the battery voltage is kept stable and without any variation (Fig. 14a) and the grid current is regulated to be a sinusoidal waveform and in phase with the grid voltage (Fig. 14b) are demonstrated clearly good dynamic performances of the proposed control scheme.

VI. CONCLUSIONS

In this paper, an effective control scheme for an EVs charging system was presented. By regulating the input current to be in phase with fundamental component of the grid voltage, the charging system injects zero harmonics current to the utility and achieves near-unity power factor. As a result, the potential harmful effects of EVs battery charger on the distribution system will be rejected. Furthermore, by adding a feed-forward voltage component to the charging algorithm, the overall dynamic response of the charging system is enhanced significantly. Finally, the simulation and experiment are carried out to verify effectiveness of the proposed control scheme.

The control scheme can be utilized in charging systems, which adopt other front-end PFC converters such as the PFC buck-based topology or the PFC symmetrical bridgeless boost rectifier-based configuration.

ACKNOWLEDGMENT

This work was partly supported by the NRF grant funded by the Korea government (MEST) (No. 2010-0025483) and the Network-based Automation Research Center (NARC) funded by the Ministry of Knowledge Economy.

REFERENCES

[1] A. Emadi, Y. J. Lee, and K. Rajashekara, "Power Electronics and Motor Drives in Electric, Hybrid Electric, and Plug-In Hybrid Electric Vehicles," *IEEE Trans. Ind. Electron,* Vol. 55, No. 6, pp. 2237–2245, Jun. 2008.

[2] O. Onar and A. Khaligh, "Grid Interactions and Stability Analysis of a Distribution Network with Plug-in Hybrid Electric Vehicle (PHEV) Loads," *IEEE-2010 Applied Power Electronics Conference and Exposition (APEC)*, pp. 1755–1762, Feb. 2010.

[3] J. R. Pillai and B. B. Jensen, "Impacts of Electric Vehicle Loads on Power Distribution Systems," *IEEE-2010 Vehicle Power and Propulsion Conference (VPPC)*, pp. 1-7, Sept. 2010.

[4] J. C. Gomez and M. M. Morcos, "Impact of EV Battery Chargers on The Power Quality of Distribution Systems," *IEEE Trans. Power Del.*, Vol. 18, No. 3, pp. 975–981, Jul. 2003.

[5] R. Liu, L. Dow, and E. Liu, "A Survey of PEV Impacts on Electric Unities," *Innovative Smart Grid Technologies (ISGT) 2011 IEEE PES*, pp. 1-8, Jan. 2011.

[6] M. M. Morcos, C. R. Mersman, G. D. Sugavanam, and N. M. DiHman, "Battery Chargers for Electric Vehicles," *IEEE Power Engineering Review,* pp. 8-11, Nov. 2000.

[7] K. W. Klontz, A. Esser, P. J. Wolfs, and D. M. Divan, "Converter Selection for Electric Vehicle Charger Systems with a High-Frequency High Power Link," *in Power Electronics Specialists Conf.,* pp. 855–861, Jun. 1993.

[8] D. Jackson, A. Schultz, S. B. Leeb, A. Mitwalli, G. Verghese, and S.R. Shaw, "A Multirate Digital Controller for a 1.5-kW Electric Vehicle Battery Charger," *IEEE Trans. Power Electron.,* Vol. 12, pp. 1000–1006, Nov. 1997.

[9] M. K. H. Cheung, M. H. L. Chow, and C. K. Tse, "Practical design and evaluation of a 1 kW PFC power supply based on reduced redundant power processing principle," *IEEE Trans, Ind. Electron.*, vol. 55, no. 2, pp. 665-673, Feb. 2008.

[10] O. L. González and G. Buja, "Novel PLL Scheme for Grid Connection of Three-Phase Power Converters," *IEEE Symposium on Diagnostics for Electrical Machines, Power Electronics & Drives 2011,* pp.372-377, Sept. 2011.

[11] T. Shimada and K. Hurokawa, "Modeling Method for Lead-Acid Battery Simulation Using Step Changing Current", *Electrical Engineering in Japan,* Vol. 128-B, No. 8, pp. 1027–1034, Aug. 2008.